



*Supplement of*

## **Real-time measurements of secondary organic aerosol formation and aging from ambient air in an oxidation flow reactor in the Los Angeles area**

**A. M. Ortega et al.**

*Correspondence to:* J. L. Jimenez ([jose.jimenez@colorado.edu](mailto:jose.jimenez@colorado.edu))

The copyright of individual parts of the supplement might differ from the CC-BY 3.0 licence.

1  
2  
3  
4  
5  
6  
7  
8  
9  
10  
11  
12  
13  
14  
15  
16  
17  
18  
19  
20  
21  
22

## **1 Quantification of AMS Reactor Data**

All aspects of quantification of AMS data are the same as described by Hayes et al. (2013). Here we describe only those aspects where additional analysis or corrections are needed specifically for the reactor output data.

### **1.1 AMS Collection Efficiency**

Quantification of AMS concentration data requires a correction for particle bounce at the vaporizer, referred to as the collection efficiency (CE; Canagaratna et al., 2007). The composition-dependent CE formulation of Middlebrook et al. (2012) was used by Hayes et al. (2013) to estimate CE for the ambient data, leading to good intercomparisons with multiple collocated instruments as documented by that study. The same methodology has also been applied to reactor output measurements.

Fig. S1a shows the time series of reactor and ambient aerosol concentrations and estimated CE. Ambient CE periodically rises above 0.5 due to larger fractions of ammonium nitrate aerosol, which leads to reduced particle bounce (Middlebrook et al., 2012). The reactor typically formed additional ammonium sulfate and ammonium nitrate beyond ambient concentrations at the same time as ambient levels peak for those compounds, thus the reactor CE profile has a very similar temporal structure to ambient. However, Fig. S1b shows that the estimated CE increases at the highest reactor  $OH_{exp}$ , due to additional ammonium nitrate formation in the reactor with increased photochemical age.

Highly acidic particles, as indicated by the ammonium balance, can also lead to increased CE in the AMS (Middlebrook et al., 2012). The ammonium balance method compares the measured

23 ammonium to that required to fully neutralize observed sulfate, nitrate, and chloride (Zhang et al.,  
24 2007), as shown in Fig. S2. Ambient and reactor results have near identical slopes that are  
25 indistinguishable from the one-to-one line within the uncertainties of the measurements, signifying  
26 full neutralization for both. Furthermore, this comparison indicates that the reactor is producing  
27 similar inorganic composition to that observed in the atmosphere as nitric acid and sulfuric acid  
28 gases are formed in the reactor and fully neutralized by ammonium forming ammonium nitrate  
29 and ammonium sulfate. Thus no correction of CE due to the presence of highly acidic particles are  
30 needed in this study.

31 Comparison of AMS and SMPS measurements for ambient and reactor data, shows that ambient  
32 data falls along a one-to-one line, indicating both instruments are measuring the same amount of  
33 mass within the uncertainties ( Fig. S3a). Reactor output data has a slightly higher slope of 1.14,  
34 i.e. the AMS measures ~14% higher mass than the SMPS from the reactor and also shows a cluster  
35 of points where  $SMPS > AMS$  due to periods where substantial mass is formed at small particle  
36 sizes (see below). Both slopes are within the combined uncertainties of the two measurements.  
37 Fig. S3b shows the relative increase in aerosol concentration in the reactor (i.e. ratio of reactor to  
38 ambient concentrations) for the SMPS vs. AMS which also compare well, on average (slope =  
39 1.05), but with considerable scatter, most of which is likely due to additional measurement noise  
40 introduced from ratioing multiple short measurements. Evaporation of freshly formed  $NH_4NO_3$  in  
41 the longer residence times in the SMPS (compared to the faster AMS analysis) where the sheath  
42 flow may have reduced  $NH_3$  and  $HNO_3$  gas concentrations, has been observed with this  
43 experimental setup, and may be a cause of the slightly larger slope for reactor output conditions.  
44 An small underestimation of AMS CE for the reactor conditions could also result in this  
45 observation.

46 It is also possible that the AMS relative ionization efficiency (RIE) of organic species is lower for  
47 more oxidized species (Jimenez et al., 2003; D. Murphy, pers. Comm. 2015), although no clear  
48 evidence has been reported for ambient data (e.g. Docherty et al., 2011). If that effect played a  
49 dominant role here, we would expect the reactor slopes to be lower, rather than slightly higher than  
50 1. Thus we conclude that any RIE changes are small and cannot be separated from other effects  
51 such as small changes in CE, nitrate evaporation in the SMPS, or differences in particle  
52 transmission (next section).

## 53 **1.2 Accounting for Particle Mass below the AMS Lens Transmission**

54 As the reactor exposed ambient air to high levels of OH and O<sub>3</sub>, new particle formation and growth  
55 was sometimes observed. To fully account for the mass of all particles formed in the reactor, it is  
56 necessary to quantify the mass of small particles below the AMS lens transmission size (Zhang et  
57 al., 2004). SMPS data was used to estimate the total mass concentration below the AMS size cut.  
58 First, particle transmission from plumbing line losses was corrected using the Particle Loss  
59 Calculator (von der Weiden et al., 2009) for this experimental plumbing and flowrate configuration  
60 for both reactor and ambient SMPS data, with transmission curves as shown in Fig. S4. Second,  
61 the measured SMPS mass that is below the AMS transmission curve was estimated using a  
62 published AMS lens transmission parameterization (Knote et al., 2011) multiplying the SMPS  
63 size-dependent mass by the size-dependent AMS lens fractional loss (1-transmission). Figure S5a  
64 shows a time series of estimated reactor and ambient mass missed by the AMS due to transmission  
65 losses. Since corrections needed to account for the contribution of these small sizes to total mass  
66 is small for ambient data (on average 1.7%), Hayes et al. (2013) did not apply a correction to AMS  
67 ambient data. Fig. S5b shows the estimated fraction of the reactor output mass that is below the  
68 AMS lens transmission size vs. total photochemical age in days (at OH = 1.5×10<sup>6</sup> molec. cm<sup>-3</sup>).

69 An average of 6.2% of the total reactor output mass is estimated to be below the AMS lens  
70 transmission, with no dependence on photochemical age except possibly at the highest values (>20  
71 days of age).

72 We note that the AMS measurements from the reactor may be biased ~6% low, on average, and  
73 sometimes as much as 20%. This non-measured mass likely has a large OA fraction (see Fig. S7).  
74 Thus, reactor-reported mass enhancement above ambient may be underestimated by these  
75 amounts. Given the 6.2% AMS underestimation from particle transmission of small sizes in the  
76 reactor, and the apparent 14% overestimation in the AMS vs SMPS comparison, but overall good  
77 agreement in the relative enhancement of total aerosol between both instruments, we have not  
78 corrected for these differences as the net correction would be small and within the uncertainties of  
79 the measurement, while the correction process would introduce additional noise.

80

81

## 82 **Supplementary Captions**

83 **Figure S1:** (a) Estimated AMS collection efficiency (CE) and corresponding AMS mass  
84 concentration time series for ambient and reactor data (after applying CE correction). (b)  
85 Estimated CE vs. OH exposure ( $\text{OH}_{\text{exp}}$ ) in the reactor for all reactor measurements and averages  
86 for 7% quantiles.

87 **Figure S2:** Measured vs. predicted ammonium assuming full neutralization (“Ammonium  
88 balance”) for ambient and reactor data. Linear orthogonal distance regression fit lines, slope and  
89  $R^2$  for each are also shown.

90 **Figure S3:** (a) Scatter plot of AMS mass vs. mass estimated from SMPS measurements for  
91 ambient and reactor data, with linear orthogonal distance regression fit slope and  $R^2$  for each. A  
92 one-to-one line and +/-15% region is shown for reference. (b) Relative enhancement ratio from  
93 AMS and SMPS data with raw data, 20-minute averaged smooth data, linear orthogonal distance  
94 regression, line, fit slope and  $R^2$  for each.

95 **Figure S4:** Estimated particle transmission of inlet plumbing vs. particle diameter for reactor and  
96 ambient sampling lines for both AMS and SMPS measurements, calculated using the particle loss  
97 calculator of von der Weiden et al. (2009).

98 **Figure S5:** (a) Time series of SMPS mass measured below the AMS lens transmission size for  
99 ambient and reactor measurements. (b) Percent of estimated mass not measured by AMS, due to  
100 on particle losses in sampling lines and the AMS lens transmission at small sizes, for the reactor  
101 vs. total photochemical age in days (at  $\text{OH} = 1.5 \times 10^6 \text{ molec. cm}^{-3}$ ), where all data is colored by  
102  $\Delta\text{OA}$  mass with average 5% quantiles and standard error bars.

103 **Figure S6:** Modeled fate of low volatility organic gases (LVOCs) formed in the reactor vs.  $\text{OH}_{\text{exp}}$   
104 including wall loss, reaction with OH, condensation on aerosol, and exiting the reactor, with a fit  
105 for the fraction condensing on aerosols in the reactor.

106 **Figure S7:** AMS mass size distribution (vs. vacuum aerodynamic diameter,  $d_{va}$ ) for reactor and  
107 ambient OA, averaged from 20:00 on 2 June 2010 – 00:20 on 9 June 2010 for average nighttime  
108 ambient and reactor with no internal  $\text{OH}_{\text{exp}}$  (dark reactor), and for  $\sim 3.7$  days and  $\sim 23.5$  days aging.

109 **Figure S8:** Times series of benzene, 1,3,5-trimethylbenzene, and toluene on top panel. Time  
110 series of ambient OOA, reactor OA mass enhancement, maximum reactor mass enhancement,  
111 and  $\text{O}_x$  on bottom panel.

112 **Figure S9:** Ratio of organic aerosol to excess carbon monoxide (above background) vs. total  
113 photochemical age in days (at  $\text{OH} = 1.5 \times 10^6 \text{ molec. cm}^{-3}$ ) for (a) the same data as Fig. 9,  
114 showing all data used to produce averages for quantiles of ambient and reactor vapor-loss  
115 corrected data. Also shown are the expected decays of benzene, toluene, and 1,3,5-  
116 trimethylbenzene in the reactor vs. total photochemical age in days (at  $\text{OH} = 1.5 \times 10^6 \text{ molec. cm}^{-3}$ ),  
117 using reaction rates from Atkinson et al. (2006). (b) The same data as Fig. 9, showing reactor  
118 vapor loss-corrected data, but where excess CO is decreased by reaction with OH in the reactor,  
119 including means for 12% quantiles. Results from field studies in the northeastern US and Mexico  
120 City are shown for comparison to previous observations (DeCarlo et al., 2010). A fit to the data  
121 when CO is assumed to react with OH is shown.

122 **Figure S10:** Measured oxygen added to OA in the reactor vs. total photochemical age in days (at  
123  $\text{OH} = 1.5 \times 10^6 \text{ molec. cm}^{-3}$ ), along with a log normal fit to the  $\Delta\text{Oxygen}$  data. Reactor data is  
124 colored by OA mass enhancement. The estimated number of OH collisions with OA is shown,  
125 based on the methodology outlined in appendix A of DeCarlo et al. (2008).

126 **Figure S11:** Top panel: Mass fraction remaining (MFR) for OA vs. thermal denuder  
127 temperature for this CalNex-LA dataset, using the methods described in Huffman et al. (2008;  
128 2009). Bottom panel: estimated volatility distribution of particle- and gas-phase species,

129 calculated from the thermal denuder profile using the method of Faulhaber et al. (2009), on  
130 bottom panel.

131

## 132 **References**

133 Atkinson, R., Baulch, D. L., Cox, R. A., Crowley, J. N., Hampson, R. F., Hynes, R. G., Jenkin, M. E., Rossi, M. J.,  
134 Troe, J., and Subcommittee, I.: Evaluated kinetic and photochemical data for atmospheric chemistry: Volume II: gas  
135 phase reactions of organic species, *Atmos. Chem. Phys.*, 6, 3625-4055, 10.5194/acp-6-3625-2006, 2006.

136 Canagaratna, M. R., Jayne, J. T., Jimenez, J. L., Allan, J. D., Alfarra, M. R., Zhang, Q., Onasch, T. B., Drewnick, F.,  
137 Coe, H., Middlebrook, A., Delia, A., Williams, L. R., Trimborn, A. M., Northway, M. J., DeCarlo, P. F., Kolb, C.  
138 E., Davidovits, P., and Worsnop, D. R.: Chemical and microphysical characterization of ambient aerosols with the  
139 aerodyne aerosol mass spectrometer, *Mass Spectrometry Reviews*, 26, 185-222, 10.1002/mas.20115, 2007.

140 DeCarlo, P. F., Dunlea, E. J., Kimmel, J. R., Aiken, A. C., Sueper, D., Crouse, J., Wennberg, P. O., Emmons, L.,  
141 Shinozuka, Y., Clarke, A., Zhou, J., Tomlinson, J., Collins, D. R., Knapp, D., Weinheimer, A. J., Montzka, D. D.,  
142 Campos, T., and Jimenez, J. L.: Fast airborne aerosol size and chemistry measurements above Mexico City and  
143 Central Mexico during the MILAGRO campaign, *Atmos. Chem. Phys.*, 8, 4027-4048, 10.5194/acp-8-4027-2008,  
144 2008.

145 DeCarlo, P. F., Ulbrich, I. M., Crouse, J., de Foy, B., Dunlea, E. J., Aiken, A. C., Knapp, D., Weinheimer, A. J.,  
146 Campos, T., Wennberg, P. O., and Jimenez, J. L.: Investigation of the sources and processing of organic aerosol  
147 over the Central Mexican Plateau from aircraft measurements during MILAGRO, *Atmos. Chem. Phys.*, 10, 5257-  
148 5280, 10.5194/acp-10-5257-2010, 2010.

149 Docherty, K. S., Aiken, A. C., Huffman, J. A., Ulbrich, I. M., DeCarlo, P. F., Sueper, D., Worsnop, D. R., Snyder,  
150 D. C., Peltier, R. E., Weber, R. J., Grover, B. D., Eatough, D. J., Williams, B. J., Goldstein, A. H., Ziemann, P. J.,  
151 and Jimenez, J. L.: The 2005 Study of Organic Aerosols at Riverside (SOAR-1): instrumental intercomparisons and  
152 fine particle composition, *Atmos. Chem. Phys.*, 11, 12387-12420, 10.5194/acp-11-12387-2011, 2011.

153 Faulhaber, A. E., Thomas, B. M., Jimenez, J. L., Jayne, J. T., Worsnop, D. R., and Ziemann, P. J.: Characterization  
154 of a thermodenuder-particle beam mass spectrometer system for the study of organic aerosol volatility and  
155 composition, *Atmos. Meas. Tech.*, 2, 15-31, 10.5194/amt-2-15-2009, 2009.

156 Hayes, P. L., Ortega, A. M., Cubison, M. J., Froyd, K. D., Zhao, Y., Cliff, S. S., Hu, W. W., Toohey, D. W., Flynn,  
157 J. H., Lefter, B. L., Grossberg, N., Alvarez, S., Rappenglück, B., Taylor, J. W., Allan, J. D., Holloway, J. S., Gilman,  
158 J. B., Kuster, W. C., de Gouw, J. A., Massoli, P., Zhang, X., Liu, J., Weber, R. J., Corrigan, A. L., Russell, L. M.,  
159 Isaacman, G., Worton, D. R., Kreisberg, N. M., Goldstein, A. H., Thalman, R., Waxman, E. M., Volkamer, R., Lin,  
160 Y. H., Surratt, J. D., Kleindienst, T. E., Offenberg, J. H., Dusanter, S., Griffith, S., Stevens, P. S., Brioude, J.,  
161 Angevine, W. M., and Jimenez, J. L.: Organic aerosol composition and sources in Pasadena, California, during the  
162 2010 CalNex campaign, *Journal of Geophysical Research: Atmospheres*, 118, 9233-9257, 10.1002/jgrd.50530,  
163 2013.

164 Huffman, J. A., Ziemann, P. J., Jayne, J. T., Worsnop, D. R., and Jimenez, J. L.: Development and Characterization  
165 of a Fast-Stepping/Scanning Thermodenuder for Chemically-Resolved Aerosol Volatility Measurements, *Aerosol  
166 Science and Technology*, 42, 395-407, 10.1080/02786820802104981, 2008.

167 Huffman, J. A., Docherty, K. S., Aiken, A. C., Cubison, M. J., Ulbrich, I. M., DeCarlo, P. F., Sueper, D., Jayne, J.  
168 T., Worsnop, D. R., Ziemann, P. J., and Jimenez, J. L.: Chemically-resolved aerosol volatility measurements from  
169 two megacity field studies, *Atmos. Chem. Phys.*, 9, 7161-7182, 10.5194/acp-9-7161-2009, 2009.

170 Jimenez, J. L., Jayne, J. T., Shi, Q., Kolb, C. E., Worsnop, D. R., Yourshaw, I., Seinfeld, J. H., Flagan, R. C., Zhang,  
171 X. F., Smith, K. A., Morris, J. W., and Davidovits, P.: Ambient aerosol sampling using the Aerodyne Aerosol Mass  
172 Spectrometer, *Journal of Geophysical Research-Atmospheres*, 108, 8425

173 10.1029/2001jd001213, 2003.

174 Knote, C., Brunner, D., Vogel, H., Allan, J., Asmi, A., Äijälä, M., Carbone, S., van der Gon, H. D., Jimenez, J. L.,  
175 Kiendler-Scharr, A., Mohr, C., Poulain, L., Prévôt, A. S. H., Swietlicki, E., and Vogel, B.: Towards an online-  
176 coupled chemistry-climate model: evaluation of trace gases and aerosols in COSMO-ART, *Geosci. Model Dev.*, 4,  
177 1077-1102, 10.5194/gmd-4-1077-2011, 2011.

178 Middlebrook, A. M., Bahreini, R., Jimenez, J. L., and Canagaratna, M. R.: Evaluation of Composition-Dependent  
179 Collection Efficiencies for the Aerodyne Aerosol Mass Spectrometer using Field Data, *Aerosol Science and  
180 Technology*, 46, 258-271, 10.1080/02786826.2011.620041, 2012.

181 von der Weiden, S. L., Drewnick, F., and Borrmann, S.: Particle Loss Calculator – a new software tool for the  
182 assessment of the performance of aerosol inlet systems, *Atmos. Meas. Tech. Discuss.*, 2, 1099-1141, 10.5194/amtd-  
183 2-1099-2009, 2009.

184 Zhang, Q., Jimenez, J. L., Canagaratna, M. R., Allan, J. D., Coe, H., Ulbrich, I., Alfarra, M. R., Takami, A.,  
185 Middlebrook, A. M., Sun, Y. L., Dzepina, K., Dunlea, E., Docherty, K., DeCarlo, P. F., Salcedo, D., Onasch, T.,  
186 Jayne, J. T., Miyoshi, T., Shimojo, A., Hatakeyama, S., Takegawa, N., Kondo, Y., Schneider, J., Drewnick, F.,  
187 Borrmann, S., Weimer, S., Demerjian, K., Williams, P., Bower, K., Bahreini, R., Cottrell, L., Griffin, R. J.,  
188 Rautiainen, J., Sun, J. Y., Zhang, Y. M., and Worsnop, D. R.: Ubiquity and dominance of oxygenated species in  
189 organic aerosols in anthropogenically-influenced Northern Hemisphere midlatitudes, *Geophys. Res. Lett.*, 34,  
190 L13801, 10.1029/2007gl029979, 2007.

191 Zhang, X. F., Smith, K. A., Worsnop, D. R., Jimenez, J. L., Jayne, J. T., Kolb, C. E., Morris, J., and Davidovits, P.:  
192 Numerical characterization of particle beam collimation: Part II - Integrated aerodynamic-lens-nozzle system,  
193 *Aerosol Science and Technology*, 38, 619-638, 10.1080/02786820490479833, 2004.

194

195



Figure S1.

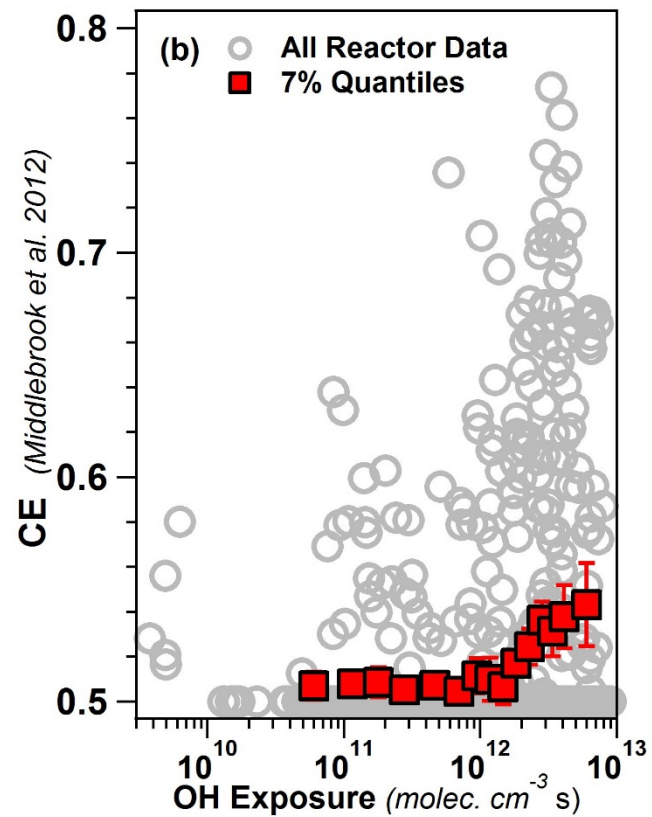
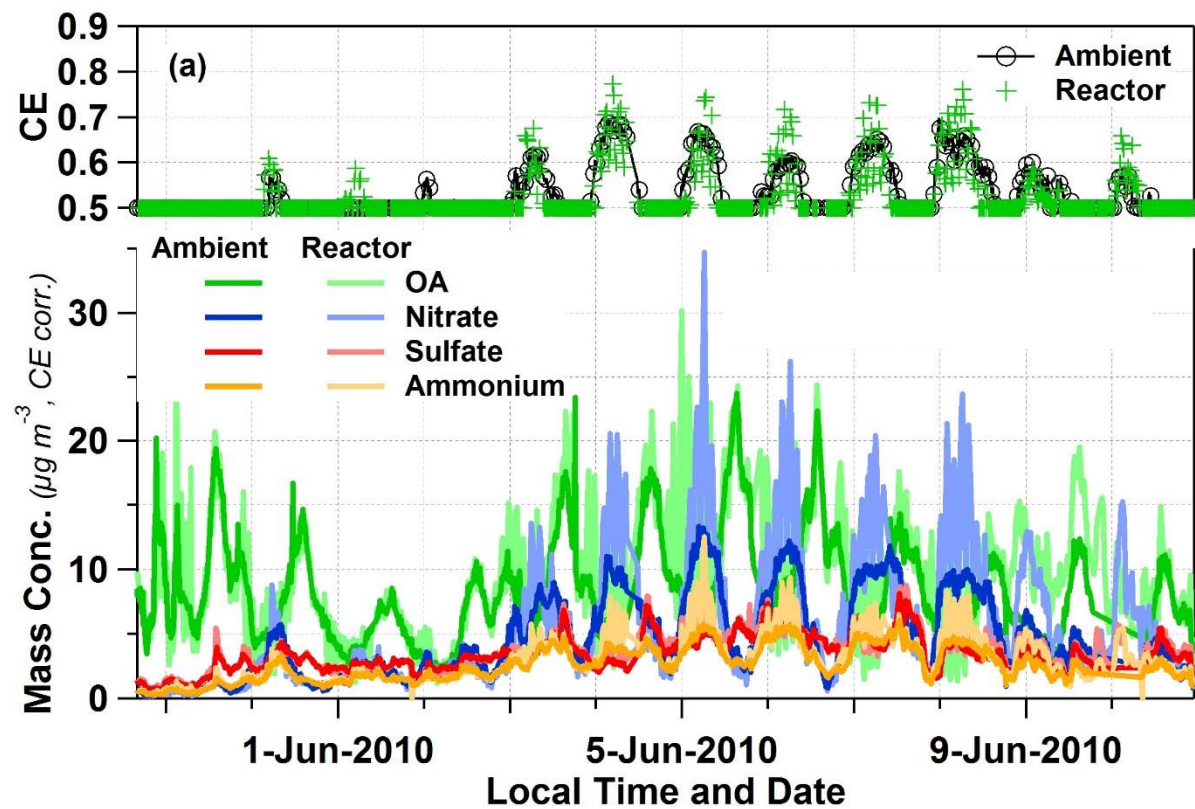


Figure S2.

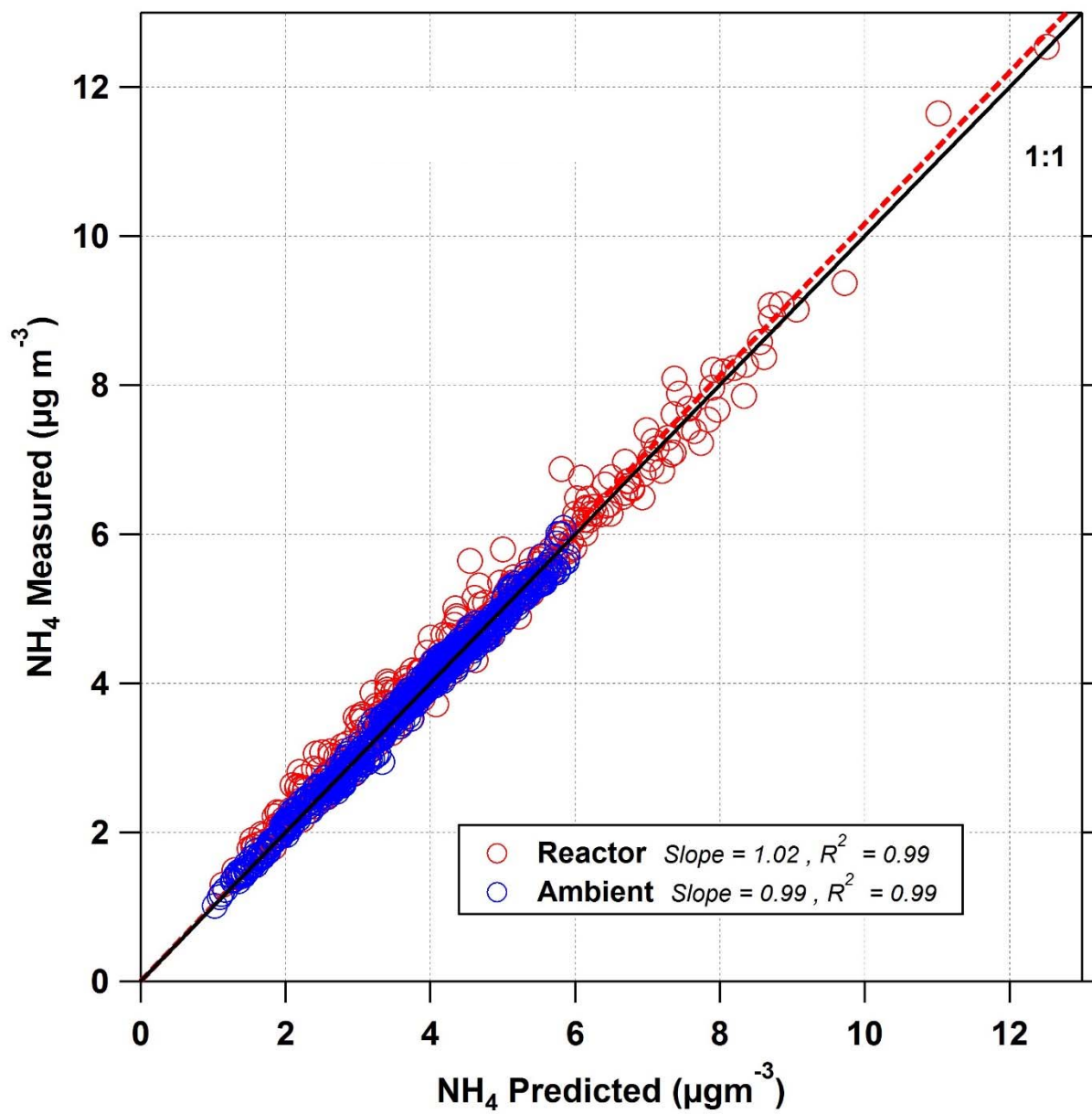


Figure S3.

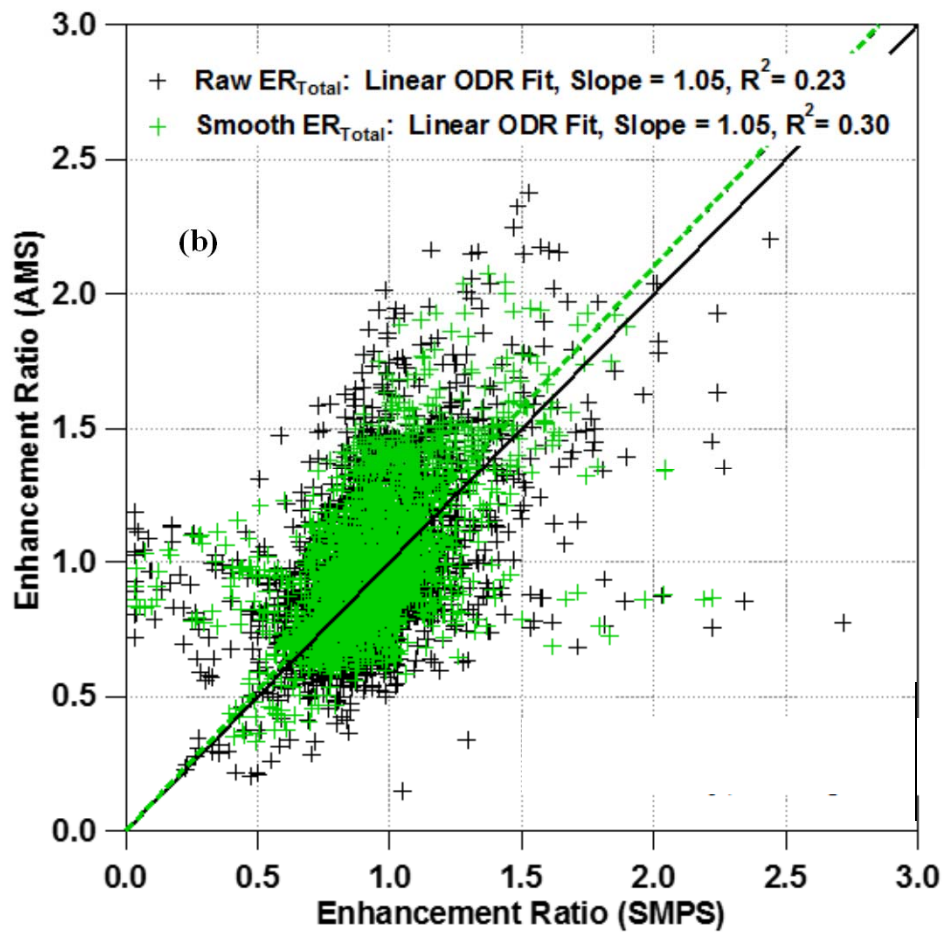
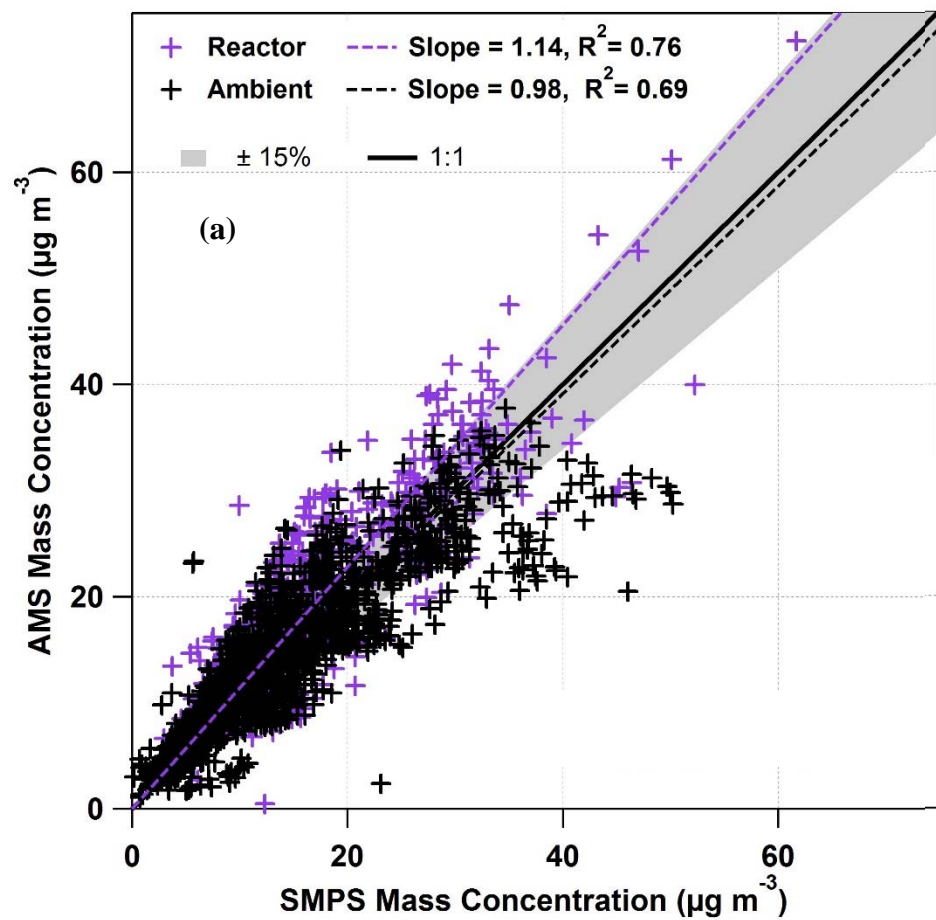


Figure S4.

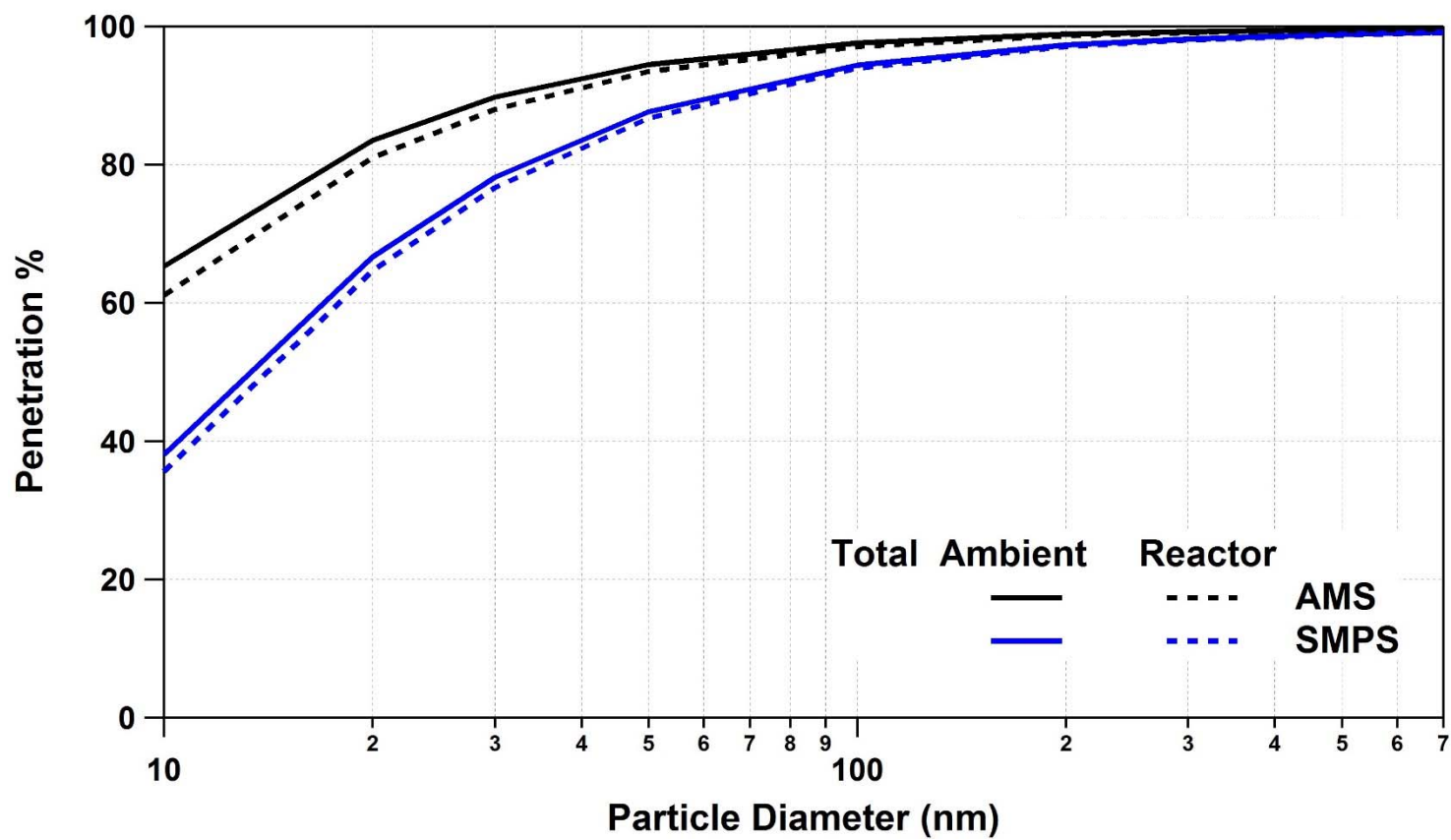


Figure S5.

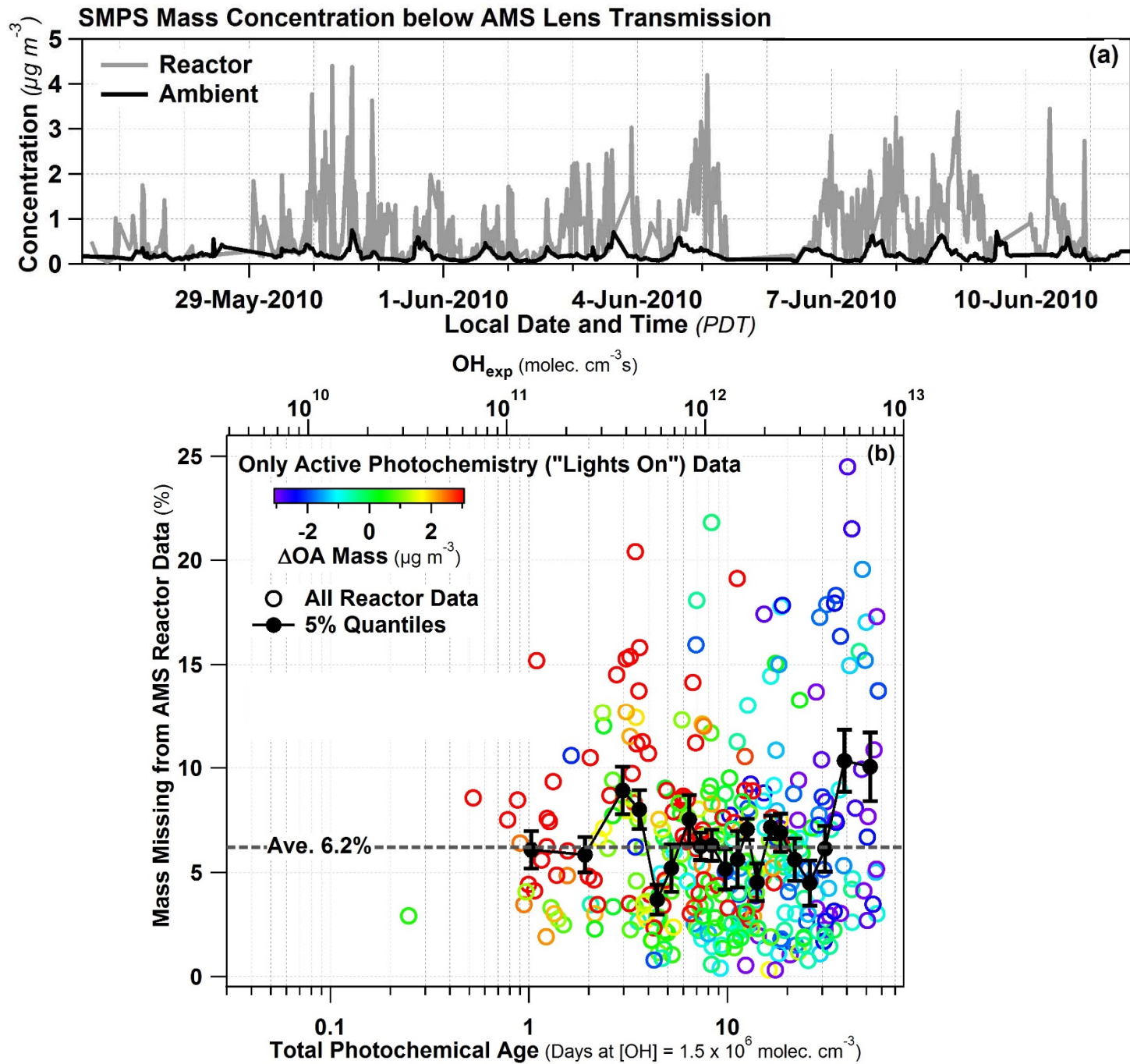


Figure S6.

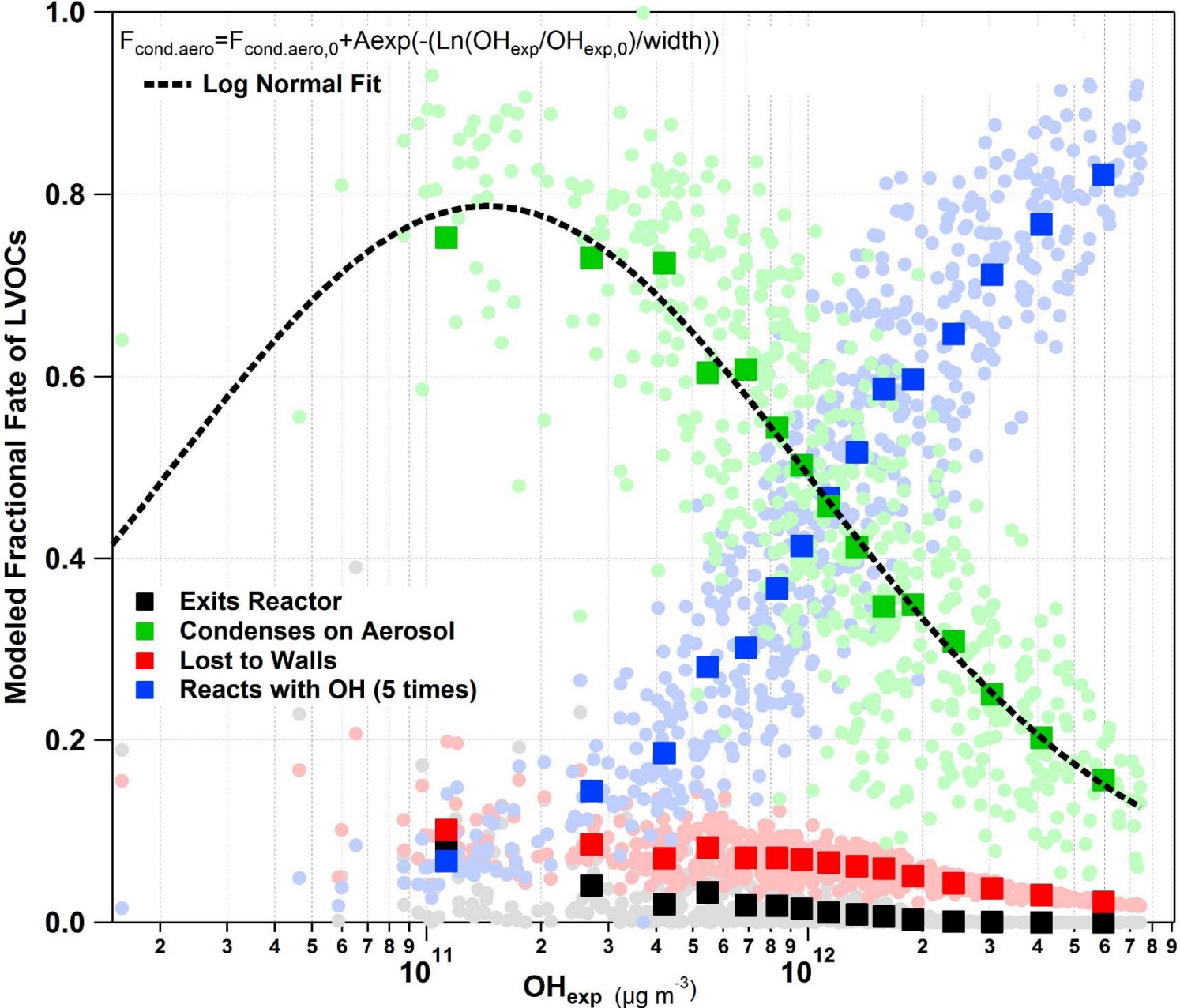


Figure S7.

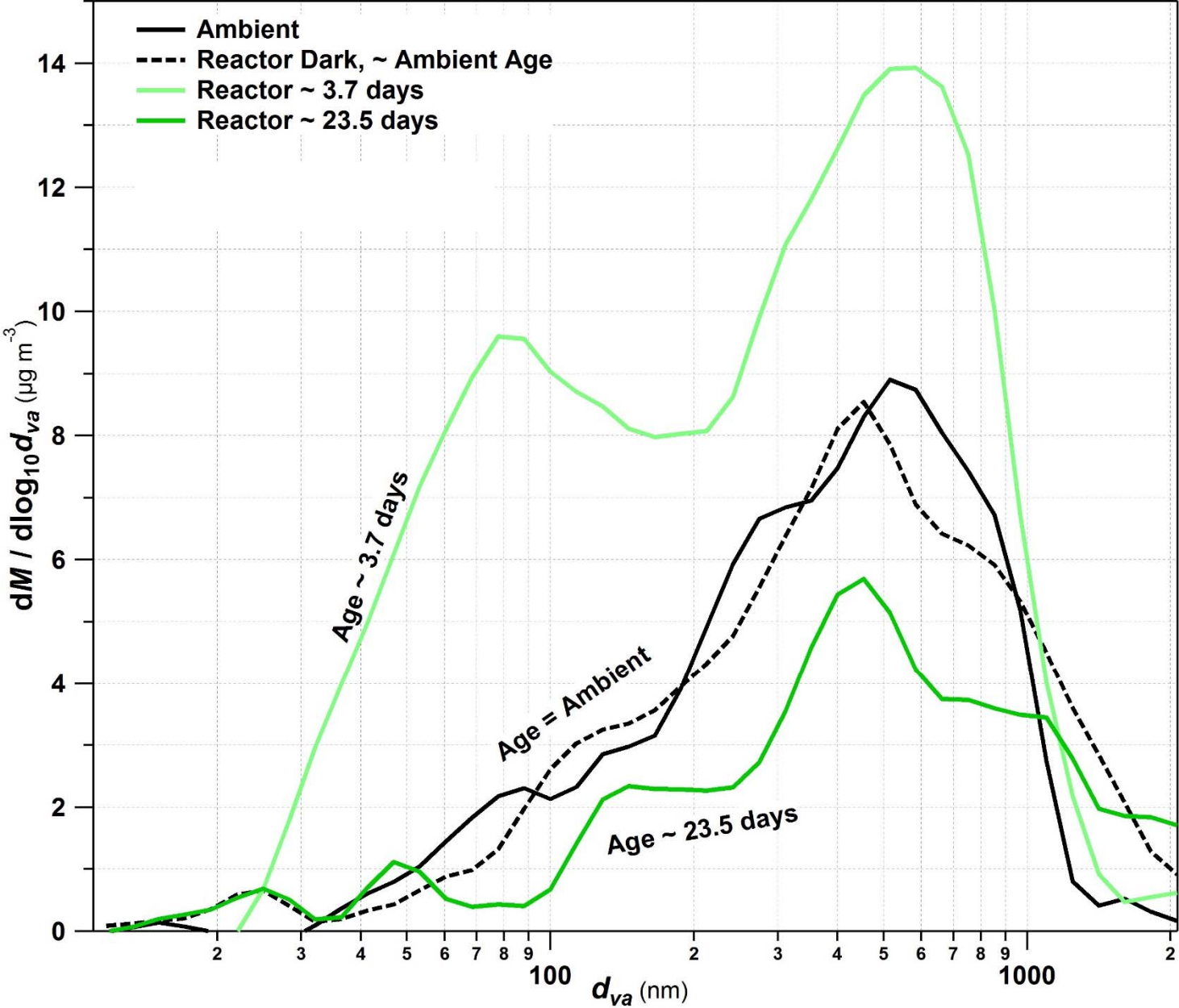
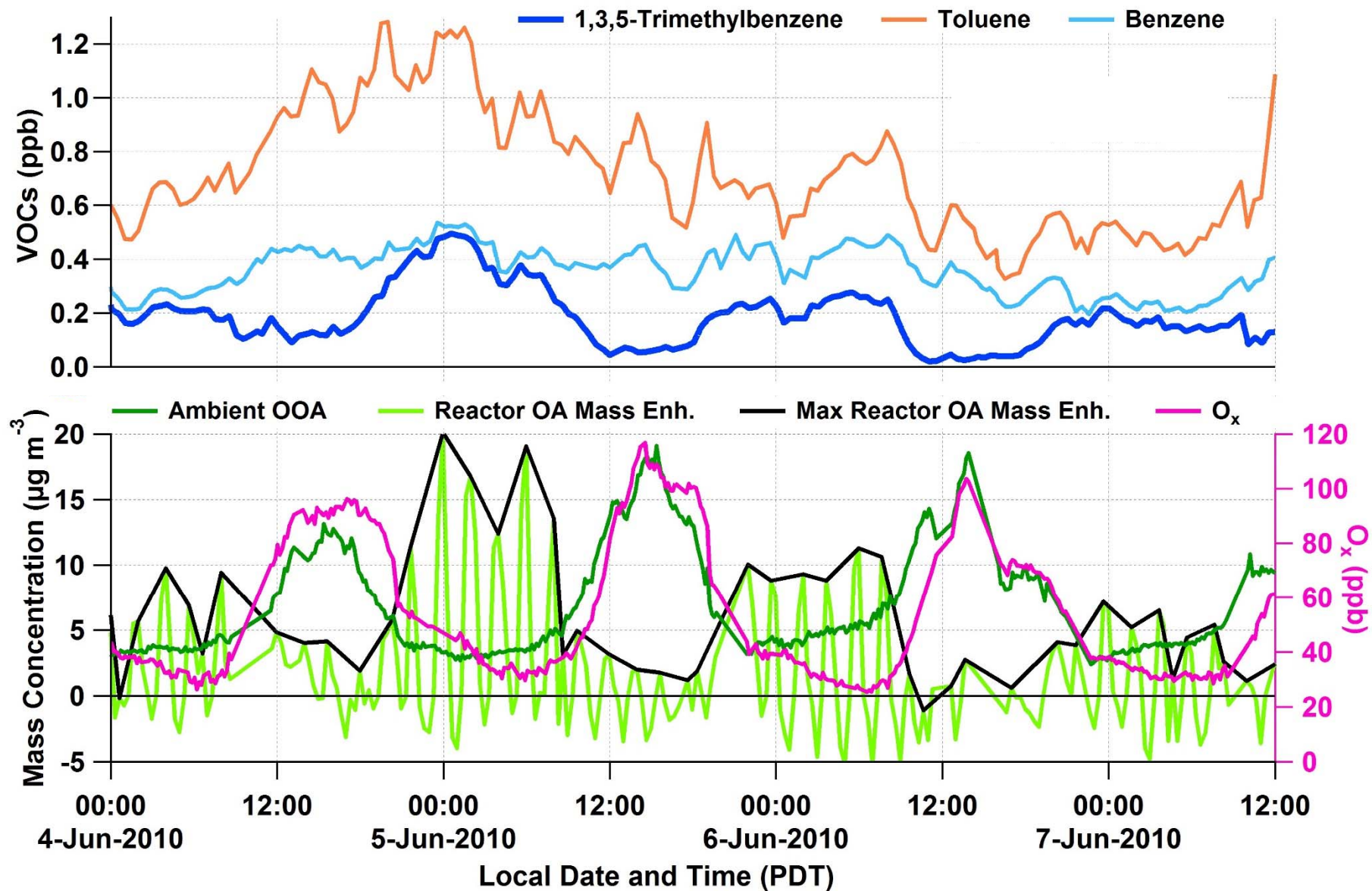
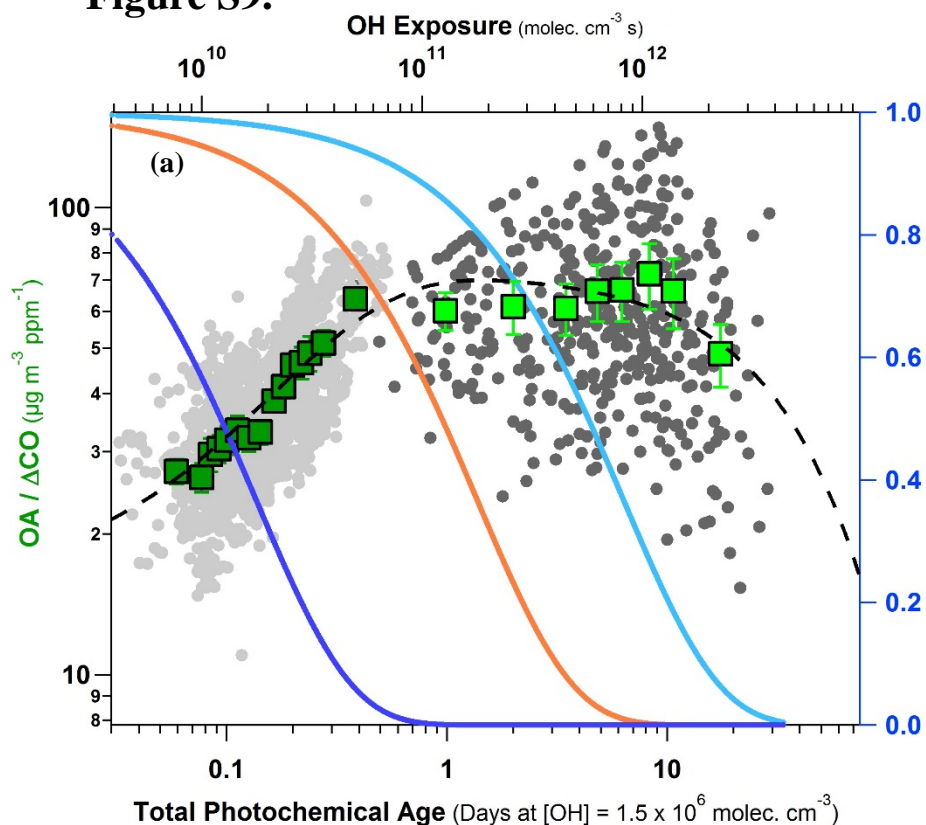


Figure S8.

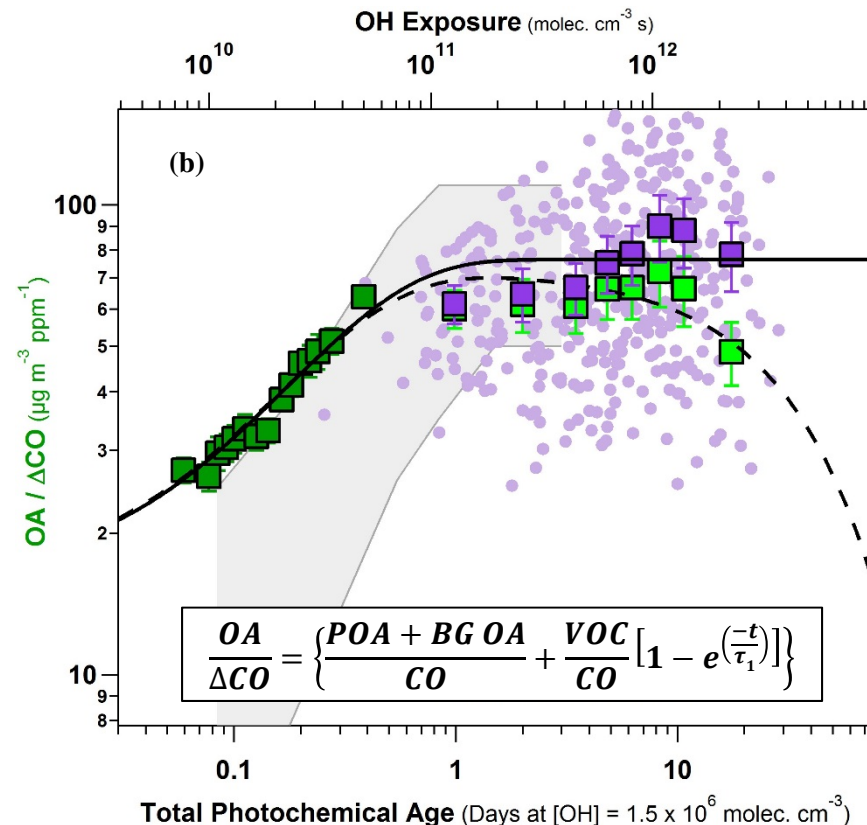




**Figure S9.**



- Ambient Data (7%) (Hayes et al. 2013)
- All Data
- Reactor (12%) Vapor Loss Corrected
- All Data
- Ambient + Reactor Fit Vapor Loss Corrected
- Trimethylbenzene
- Toluene
- Benzene



- Ambient Data (7%) (Hayes et al. 2013)
- Reactor (12%) Vapor Loss Corrected
- Ambient + Reactor Fit Vapor Loss Corrected
- All CO-reacted Data
- Reactor CO-reacted (12%)
- Ambient + Reactor CO-reacted Fit
- Northeast US & Mexico City (DeCarlo et al. 2010)

$$\frac{POA+BG\ SOA}{CO} = 16 \frac{\mu g}{m^3 ppm}$$

$$\frac{VOC^*}{CO} = 60 \pm 5 \frac{\mu g}{m^3 ppm}$$

$$\tau_1 = 0.3 \pm 0.1 \text{ days}$$

$$\frac{OA}{\Delta CO} = \left\{ \frac{POA + BG\ OA}{CO} + \frac{VOC}{CO} [1 - e^{(-t/\tau_1)}] \right\}$$

Figure S10.

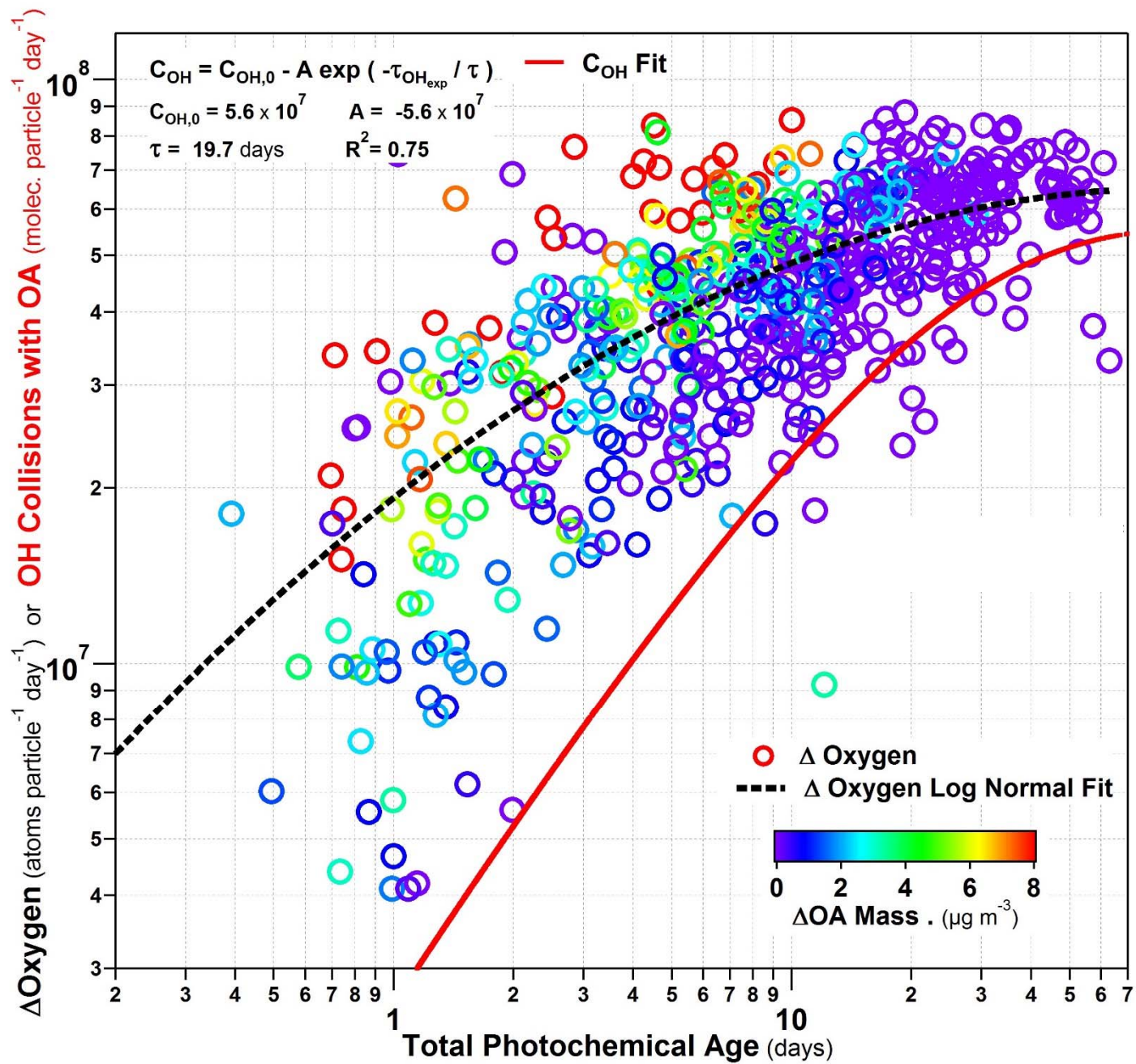


Figure S11.

